PERFORMANCE CHARACTERIZATION OF VEHICULAR VISIBLE LIGHT COMMUNICATIONS

A Thesis

by

Mehdi Karbalay Ghareh

Submitted to the

Graduate School of Sciences and Engineering
In Partial Fulfillment of the Requirements for
the Degree of

Master of Science

in the
Department of Electrical and Electronics Engineering

Özyeğin University
July 2019

PERFORMANCE CHARACTERIZATION OF VEHICULAR VISIBLE LIGHT COMMUNICATIONS

Approved by:

Professor Murat Uysal, Advisor,
Department of Electrical and
Electronics Engineering
Ozyegin University

Assistant Professor Kadir Durak,
Department of Electrical and
Electronics Engineering
Ozyegin University

Assistant Professor Bahattin Karakaya,
Department of Electrical and
Electronics Engineering
Istanbul University

Date Approved: 16 July 2019

To my dear parents

ABSTRACT

In Intelligent Transportation Systems (ITSs), visible light communication (VLC) has emerged as a powerful candidate to enable wireless connectivity in vehicle-to-vehicle (V2V) and vehicle-to-infrastructure (V2I) links. VLC has been proposed as an alternative or complementary technology to radio frequency vehicular communications. While VLC has been studied intensively in the context of indoor communications, its application to vehicular networking is relatively new. Light emitting diodes (LEDs) are increasingly used in automotive exterior lighting. The expected wide availability of LED-based front and back lights makes VLC a natural vehicular connectivity solution. A major challenge in vehicular VLC systems is their relatively poor performance in adverse weather conditions such as severe fog. In this thesis, we evaluate the performance limits of vehicular VLC systems.

In the first part of this thesis, we determine the maximum achievable distance to ensure a given bit error rate (BER) assuming positive-intrinsic-negative (PIN) diode as a receiver. We further investigate the deployment of relay-assisted systems to extend transmission ranges. In the second part of this thesis, we propose the use of single-photon avalanche diode (SPAD) for vehicular VLC systems. With their higher sensitivity in comparison to conventional photodetectors, SPADs can be efficiently used to detect weak signals. Under the assumption of on-off keying (OOK), we present the error rate performance of vehicular VLC systems. Since the SPAD output is modelled by Poisson statistics, BER takes the form of a semi-infinite summation. Based on Anscombe transformation, we approximate Poisson noise as Gaussian and derive a closed-form BER expression. Using this expression, we obtain a closed-form expression for maximum

achievable link distance to ensure a targeted BER. We further investigate the deployment of relay-assisted systems to extend transmission ranges. In the third part of this thesis, we propose the use of SPAD array receiver for vehicular VLC systems. We obtain the closed-form expression for maximum achievable distance to ensure targeted BER. We present an extensive numerical study to validate our derivations and demonstrate the performance of vehicular VLC systems under different weather conditions.

ÖZET

Akıllı Ulaşım Sistemlerinde (Intelligent Transportation Systems-ITS), görünür ışık haberleşmesi (visible light communication-VLC), araçtan araca (vehicle-to-vehicle—V2V) ve araçtan altyapıya (vehicle-to-infrastructure—V2I) bağlantılarda kablosuz bağlantı sağlamak için güçlü bir aday olarak ortaya çıkmıştır. VLC, radyo frekansı araç iletişimine alternatif veya tamamlayıcı bir teknoloji olarak önerilmiştir. VLC, iç iletişim bağlamında yoğun bir şekilde çalışılsa da, araç ağlarına uygulanması nispeten yenidir. Işık yayan diyotlar (Light emitting diodes-LEDs), otomobil dış aydınlatmasında giderek daha fazla kullanılmaktadır. LED tabanlı ön ve arka ışıklardan beklenen geniş kullanılabilirlik, VLC doğal bir araç bağlantı çözümü yapar. Araç VLC sistemlerindeki en büyük zorluk, şiddetli sis gibi olumsuz hava koşullarında nispeten düşük performans göstermeleridir. Bu tezde araç VLC sistemlerinin performans sınırlarını değerlendirdik.

Bu tezin ilk kısmında, alıcı olarak PIN diyotu varsayarak verilen bit hata oranını (bit error rate-BER) sağlamak için ulaşılabilecek maksimum mesafeyi belirliyoruz. İletim aralıklarını genişletmek için röle destekli sistemlerin dağıtımını daha da araştırıyoruz. Bu tezin ikinci kısmında, araç VLC sistemleri için tek foton çığ diyotu (single-photon avalanche diode-SPAD) kullanılmasını öneriyoruz. Geleneksel fotodedektörlere kıyasla daha yüksek hassasiyetleri ile SPAD'ler zayıf sinyalleri tespit etmek için verimli bir şekilde kullanılabilir. Açma-kapama anahtarlama varsayımı altında, araç VLC sistemlerinin hata oranı performansını sunuyoruz. SPAD çıktısı Poisson istatistiklerine göre modellendiğinden, BER yarı sonsuz bir toplamı oluşturur. Anscombe dönüşümüne dayanarak, Poisson gürültüsünü Gauss kadar yaklaştırarak kapalı bir BER ifadesi elde

ediyoruz. Bu ifadeyi kullanarak, hedeflenen bir BER'i sağlamak için ulaşılabilir maksimum bağlantı mesafesi için kapalı formlu bir ifade elde ediyoruz. İletim aralıklarını genişletmek için röle destekli sistemlerin dağıtımını daha da araştırıyoruz. Bu tezin üçüncü kısmında, araç VLC sistemleri için SPAD dizi alıcının kullanılmasını öneriyoruz. Hedeflenmiş BER'i sağlamak için kapalı form ifadesini ulaşılabilecek maksimum mesafe için elde ederiz. Türevlerimizi doğrulamak ve farklı hava koşullarında araç VLC sisteminin performansını göstermek için kapsamlı bir sayısal çalışma sunuyoruz.

ACKNOWLEDGMENTS

I would like to express my utmost gratitude to my supervisor, Professor Murat Uysal, for his excellent guidance, motivation and immense knowledge. This thesis would have not been possible without his consistence support throughout the course of my M.Sc. studies. I consider it an honor to work with him. I will never forget his support and for providing me numerous opportunities to learn and develop as a researcher.

I would also like to sincerely acknowledge the members of my thesis committee, Dr. Kadir Durak and Dr. Bahattin Karakaya for their time serving on my committee and carefully reviewing my thesis.

Last, but not least, I owe my deepest gratitude to my dear parents and my brother for their endless love and sincere encouragement and inspiration throughout my life.

TABLE OF CONTENTS

LIST OF TABLES

LIST OF FIGURES

CHAPTER I

INTRODUCTION

1.1 Motivation

Building upon cooperation, connectivity, and automation of vehicles, Intelligent Transportation Systems (ITSs) are expected to improve road safety, traffic efficiency and comfort of driving [1]. The efficient and timely information flow in ITSs becomes possible through vehicle-to-vehicle (V2V), vehicle-to-infrastructure (V2I) and infrastructure-to-vehicle (I2V) communications, sometimes collectively referred to as V2X communications. Ongoing research activities and standardization efforts have mainly considered radio frequency (RF) wireless access technologies for V2X communications [2, 3]. The IEEE 802.11p standard was approved back in 2010 and defines enhancements to 802.11 required to support ITS applications. In 2017, LTE-Vehicle (LTE-V) was introduced as a part of 3GPP Release 14 [4].

Since the market penetration is currently low, the spectrum of RF has low usages for the impact of V2X communications. However, it is expected to significantly increase with the widespread adaptation of ITSs. In RF-based V2X communications, the fulfilling of the scalability, reliability, demanding latency, and the requirements of capacity in vehicular networks can be considered as major challenges. It should be noted that, the interference levels of RF systems are almost high in replete environments. In addition, RF systems have longer delays and lower packet rate due to the fact that the channel is congested. To address such issues, visible light communication (VLC) has been proposed

that can be used as an alternative or complement to RF-based vehicular connectivity [5-7]. In VLC, the light of light emitting diode (LED) is modulated at so high speeds which cannot be noticed by human eye. Visible band (400-700 nm) is used as a carrier for the information transmission, and thus it has larger bandwidth in compare to the RF systems. In addition, the spectrum of visible light is not ordered and thus the technology's expense is greatly decreased. The vast spectrum of visible light empowers VLC to attain so high information rates which can climb to the order of Gb/s [8, 9]. Therewith, since this information rate has been immediately attained after the start of the development of the VLC systems, it is clear that the potential of this technology is very high. With these characteristics, VLC can truly be a part of future high speed data transmissions [10-13]. VLC is quite compatible to RF systems as well, therefore, both of them can integrate each other, making heterogeneous or hybrid networks as well as improving the performance of data transmissions [13, 14].

In terms of human health, VLC is so safe in compared to other wireless communication technologies and it can be considered as an significant advantage of VLC. For the sake of comparison, the RF waves are recently known as a possible cause of some human diseases such as cancer [15-18], whilst the infrared (IR) light could be very harmful for the cornea. In addition, VLC systems can be efficiently applied for the RF limited places such as hospitals. Furthermore, due to the increasing interest to decrease greenhouse emissions, the efficiency of energy in VLC is also very high, since it does not use extra energy for information transmission. In other words, the same light is utilized for both information transmission and illumination.

A main difference between VLC and RF communications comes from the inherent properties of the exploited electromagnetic waves. The RF waves have the ability

to penetrate through most nonmetallic materials, whereas the visible light can only penetrate through transparent materials. Even though in some cases, the limited penetration capability acts as a disadvantage by limiting the mobility or the coverage area, it could also represent a major benefit, since it limits the interferences between the non-line-of-sight (NLOS) systems and prevents eavesdropping.

In addition to the aforementioned benefits, one of the greatest advantages of VLC is the ubiquitous character. In VLC, the information transmission capacity is enabled by fast switching LEDs, as an additional function besides lighting. Thus, the information is transmitted onto the instantaneous power of the light, at speeds unperceivable by the human eye. Since new generation vehicles are typically fitted with LED-based front and back lights, VLC becomes a natural vehicular connectivity solution based on the dual use of LEDs in addition to their primary illumination function. The efficiency of the LEDs made them being used for LED-based traffic lights as well. This new generation of LED-based traffic lights is rapidly gaining popularity and its usage on extended scale is only straightforward. These traffic lights have as advantages a low maintenance cost, long life and low energy consumption and also offer a better visibility. While some of the cities authorities have already replaced the classical traffic lights with LED-based traffic lights, other cities are progressively following this trend.

Considering the trends in the lighting industry, it is expected that in the near future, street lighting will be LED-based as well. Therefore, with the help of the VLC technology, the road illumination will also be able to provide communication support as in [19] and [20]. In such a case, the constant short distance between the street light and vehicles, along with the high power implied, enables high data rates and increased communication stability. Under these circumstances, this particular case of I2V VLC has

a huge developing potential. Moreover, due to the low-cost and high reliability, LEDs begun to be integrated in traffic signs as well, in order to improve the visibility. Currently, this type of traffic signs are used mainly on the road segments which are considered with a high accident risk.

Considering the upper mentioned context, one can see that LED-based lighting will be part of the transportation system, being integrated in vehicles and also in the infrastructure. The large geographical area in which LEDs lighting will be used, combined with VLC technology will allow ITS to gather information from a widespread area and thus, the VLC technology can enable widespread distribution of high quality communications. The success of the ITS is largely dependent on its penetration. Insufficient penetration means insufficient information collection and distribution. If it is to think of RF solutions for the ITS, this will not be possible for a long time ahead because, in order the system to be effective, it is needed that all intersection and streets to be equipped with RF units, which implies a huge implementation cost. Hence, one of the strongest advantages of VLC is its low complexity and the reduced implementation cost. Being already half integrated in the existing transportation infrastructure, as well as in vehicle lighting systems, makes VLC a ubiquitous technology and ensures it a fast market penetration. Additionally, the vehicles are able to exchange data concerning their state (e.g., location, velocity, acceleration, engine state, etc.). In the case of RF, the problem of market penetration is considered a serious issue that can block the deployment. It is estimated that in order for such a system to begin being effective it requires at least a 10% market penetration [21]. However, to achieve this, it would require a few years in which 5 the system brings little or no benefits, meaning that the deployment cost is mostly

supported by the early buyers. Notwithstanding that a significant part of the consumers replace the car in this period without having any benefit from the purchased system.

There is a growing literature on vehicular VLC addressing a wide range of topics such as channel modeling, physical layer design, networking aspects as well as integration with RF-based solutions for hybrid solutions, see e.g., a recent survey in [22] and the references therein. In the VLC system, either a photodetector or imaging sensor (i.e., camera) can be used at the receiver side to extract the data from the modulated light beam. While the on-board cameras are able to support very low data rates due to the limited number of frames per second, photodiode (PD)-based receivers can support much higher rates. Several works in the literature have investigated the performance of vehicular VLC system assuming the deployment of positive-intrinsic-negative (PIN) diodes and avalanche photo diodes (APDs), see e.g., [23-25].

A major challenge in vehicular VLC systems is their relatively poor performance in adverse weather conditions such as severe fog [23, 25]. In these environments where the received optical power is weak, conventional PDs have unsatisfactory performance because high detection threshold and high noise intensity associated with trans-impedance amplifier (TIA) significantly reduce the sensitivity of the receiver and limit the signal-to-noise ratio (SNR) [26-28]. As an alternative, single-photon avalanche diode (SPAD) can be used which does not require a TIA. A SPAD is basically an APD which operates in Geiger mode. In this mode, SPAD is biased beyond reverse breakdown voltage, thus it can trigger billions of electron-hole pair generations by receiving each photon. Therefore, SPAD is very sensitive receiver and can be efficiently used to detect weak signals [28, 29].

With their superior performance, SPADs were considered as VLC receivers in the literature for harsh propagation environments such as underwater [26, 30] and gas pipelines [31]. However, their use was not investigated before in the context of vehicular VLC systems.

1.2 Thesis Outlines

In the first part of our work, we focus on the performance characterization of vehicular VLC with PIN-diode receiver. We use the expression of path loss model in [25] to determine the maximum achievable distance for point-to-point transmission under different weather conditions. To extend the transmission range, the deployment of relay-assisted vehicular VLC systems is also investigated. We consider multi-hop vehicular VLC systems where the relay nodes are located equidistant from each other and obtain the closed-form expression for maximum achievable distance to satisfy a targeted BER.

In the second part of our work, we investigate the performance of a V2V VLC system with SPAD receiver. Under OOK assumption, we first derive an approximate closed-form BER expression based on the Anscombe root transformation, i.e., approximation of the Poisson noise by square-root AWGN. Then, we obtain the maximum achievable link distance to ensure a targeted BER under various weather conditions including rain and fog. We then extend our results to multi-hop vehicular VLC systems. We further quantify performance improvements over conventional vehicular V2V VLC systems with APD receivers.

In the third and final part of our work, we investigate the performance of vehicular VLC with SPAD array receivers. We use the approximate BER expression to derive the maximum achievable distance between two vehicles under different weather conditions

while the targeted BER is satisfied. We further study the effect of channel and receiver parameters on the maximum achievable distance.

1.3 Organization

The rest of thesis is organized as follows. In Chapter II, we determine the maximum achievable distance to satisfy a targeted BER value for point-to-point and multi-hop V2V scenarios assuming PIN-diode receivers. In Chapter III**,** we derive a closed-form expression for BER assuming SPAD receivers. Then, we determine the maximum achievable distance to satisfy a targeted BER value for point-to-point and multi-hop V2V scenarios. In Chapter IV, we present a closed-form expression for maximum achievable distance between two vehicles assuming SPAD array receivers using a new path loss model for V2V communication. Finally, Chapter V concludes and summarizes this thesis.

CHAPTER II

Vehicular VLC with PIN-Diode Receivers

In this chapter, we consider a V2V VLC system where two high-beam headlamps of the first vehicle are used as transmitters (see Fig. 1). A PIN-diode receiver is placed in the back side of the other vehicle. Here, we derive a closed-form expression for maximum achievable distance between two vehicles to ensure targeted BER. We further investigate multi-hop transmission to extend transmission ranges.

2.1 System Model

We consider a V2V VLC system with PIN-diode receiver. We assume Pulse Amplitude Modulation (PAM) to modulate optical signal from LED. The electrical received signal can be written as

$$y = rP_t hT_b + w \tag{1}$$

where r is the responsivity of the photodetector. T_b is the bit time duration and w is additive white Gaussian noise (AWGN) with zero mean and variance of σ_n^2. In (1), h denotes the deterministic channel coefficient between two vehicles. According to [25], h takes the form of

$$h = 10^{\left(\frac{Ad+B}{10}\right)} \tag{2}$$

where d denotes the distance from the vehicle and A and B are weather-dependent coefficients (see Table 1).

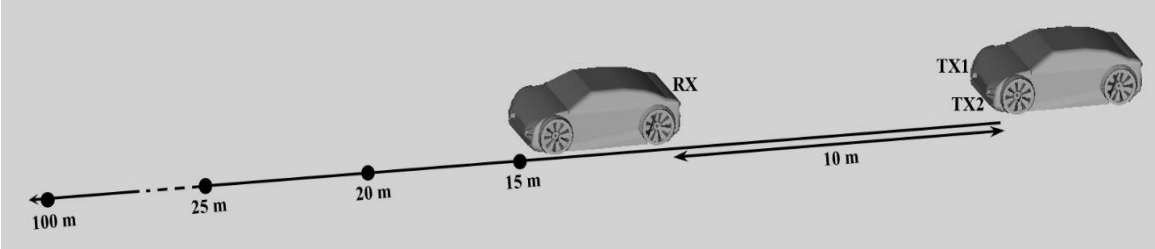

Figure 1: V2V scenario under consideration

Table 1: Coefficients in (2) for different weather types

	A	*B*
Clear	-0.44	-40.93
Rain	-0.46	-40.90
Fog, $V = 50$ m	-0.61	-40.46
Fog, $V = 10$ m	-1.20	-40.38

2.2 Maximum Achievable Distance

2.2.1 Point-to-Point Transmission

For high SNR region and over AWGN channel, the BER of *M*-ary PAM can be approximated by [32]

$$P_e \approx \frac{2(M-1)}{M\log_2(M)} Q\left(\frac{1}{M-1}\sqrt{\frac{(rhP_t)^2 T_s}{N_0}}\right) \tag{3}$$

where N_0 is the noise power spectral density. Let P_e' denote the targeted BER value. Based on (3), the required h value to achieve a given targeted BER of P_e' can be obtained as

$$h \approx \left(\frac{M-1}{rP_t}\right) Q^{-1}\left(\frac{P_e' M\log_2 M}{2(M-1)}\right)\sqrt{\frac{N_0}{T_s}} \tag{4}$$

By replacing (2) in (4), the maximum transmission distance is obtained as

$$d_{\text{PIN}} \approx \left(\frac{1}{A}\right)\left(10\log_{10}\left(\left(\frac{M-1}{rP_t}\right)Q^{-1}\left(\frac{P_e' M \log_2 M}{2(M-1)}\right)\sqrt{\frac{N_0}{T_s}}\right) - B\right) \tag{5}$$

where A and B are weather-dependent coefficients (see Table 1).

2.2.2 Multi-Hop Transmission

In this section, we explore the deployment of multi-hop transmission to extend transmission range. We assume the deployment of detect-and-forward (DF) relaying. Let N denote the number of relay terminals. Let h_i denote the optical channel coefficient for the i^{th} hop, $i = 1, \cdots, N+1$. The end-to-end BER for a DF serial relaying system is given as [33]

$$P_{e,\text{SD}} = 1 - \prod_{i=1}^{N+1}\left(1 - P_{e,i}\right) \tag{6}$$

where $P_{e,i}$ is the BER of the i^{th} hop. This can be lower bounded by [34]

$$P_{e,\text{SD}} \geq 1 - \left(1 - P_{e,\text{hop}}\right)^{N+1} \tag{7}$$

where the average BER of all hops are identical, i.e., $P_{e,i} = P_{e,\text{hop}}$, $i = 1, \cdots, N+1$. This is possible when the intermediate vehicles (serving as relay nodes) are located equidistant from each other. Noting that $\ln(1+x) \approx x$ for small x [35], $P_{e,\text{hop}}$ can be obtained as

$$P_{e,\text{hop}} \approx \frac{P_{e,\text{SD}}}{(N+1)} \tag{8}$$

Let $P_{e,\text{SD}}'$ denote the targeted value of the end-to-end BER. This indicates that

$P'_{e,\text{hop}} = P'_{e,\text{SD}} \big/ (N+1)$ should be satisfied per hop. Utilizing (8), the required h_{hop} value to achieve $P'_{e,\text{hop}}$ can be obtained. By replacing the resulting expression in (7), the maximum achievable distance per hop is calculated. Multiplying this with $(N+1)$, we obtain an approximate upper bound on the maximum achievable distance as

$$d_{\text{MH-PIN}} \lesssim (N+1)\left(\frac{1}{A}\right)\left(10\log_{10}\left(\left((M-1)\sqrt{\frac{(N+1)N_0}{(rP_t)^2 T_s}}\right)Q^{-1}\left(\frac{P'_{e,\text{SD}}\, M \log_2 M}{2(M-1)(N+1)}\right)\right)-B\right) \tag{9}$$

2.3 Numerical Results

In this section, we present numerical results for the maximum achievable link distance in point-to-point and multi-hop transmission systems under different weather types and modulation orders to achieve a specified BER. We assume $r = 0.28$ A/W [36], $P_t = 10$ dBm per each headlamp, $N_0 = 10^{-22}$ W/Hz and $T_s = 1$ msec. We set P'_e as 10^{-6}. Simulation parameters are summarized in Table 2.

Table 2: Simulation parameters

Parameters	**Values**
Responsivity of the photodetector (r)	0.28 A/W [25]
Noise power spectral density (N_0)	10^{-22} W/Hz [25]
Transmit power per each headlamp (P_t)	10 dBm
Symbol duration (T_s)	1 msec
Targeted BER (P'_e)	10^{-6}

In Figs. 2-5, we present the BER performance versus distance based on (3) for a point-to-point V2V system assuming different weather types. In Table 3, we present the maximum achievable distances based on (5) for different sizes of PAM. It is observed that the maximum distance that can be obtained for the clear weather by 2-PAM is 72.21 m. This reduces to 69.13 m, 52.85 m and 26.93 m respectively for rainy weather, foggy weather with visibility of $V = 50$ m and foggy weather with visibility of $V = 10$ m. This is a result of the fact that the light beam has more attenuation in adverse weather types. It is also observed that as modulation size is increased, the maximum distance for reliable transmission decreases. For example, for 32-PAM, the maximum distance that can be obtained for the clear weather is 38.73 m. This reduces to 37.11 m, 28.71 m and 14.66 m respectively for rainy weather, foggy weather with visibility of $V = 50$ m and foggy weather with visibility of $V = 10$ m.

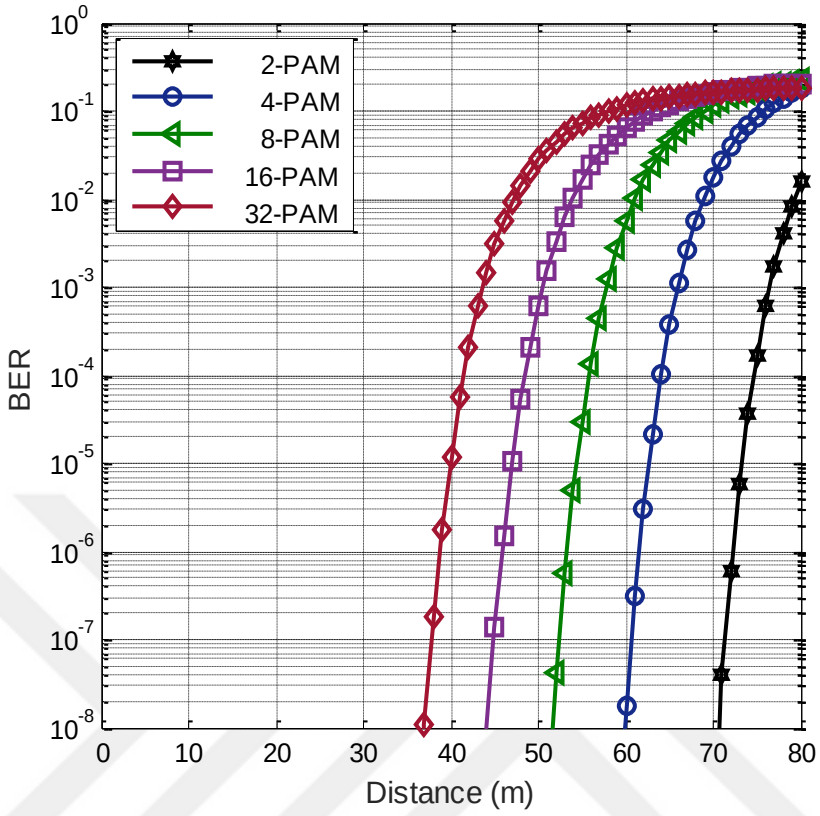

Figure 2: BER performance of V2V transmission for clear weather

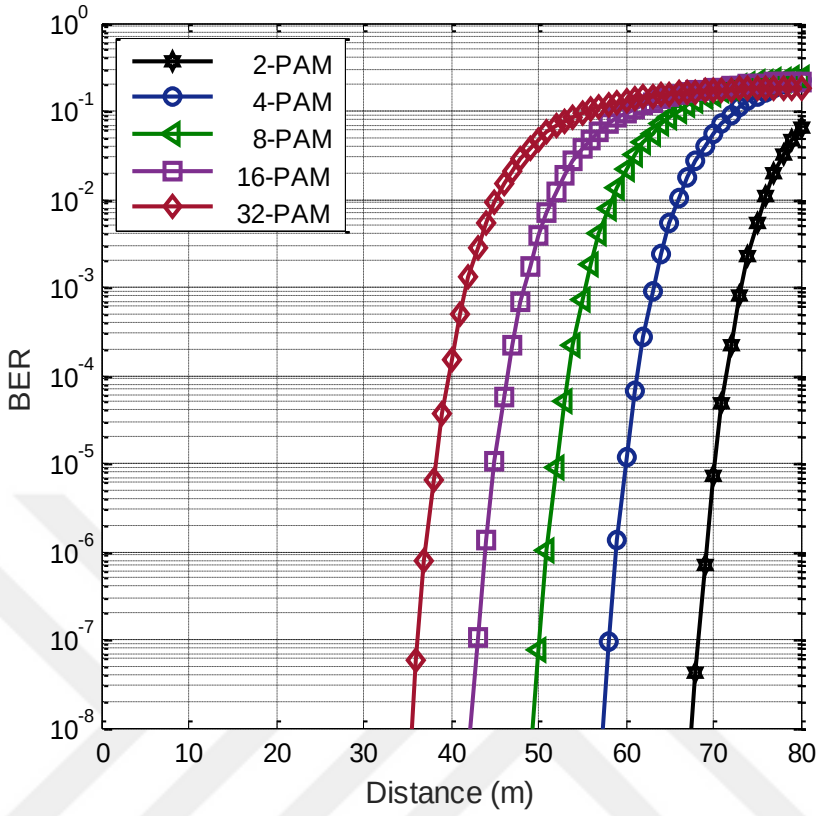

Figure 3: BER performance of V2V transmission for rainy weather

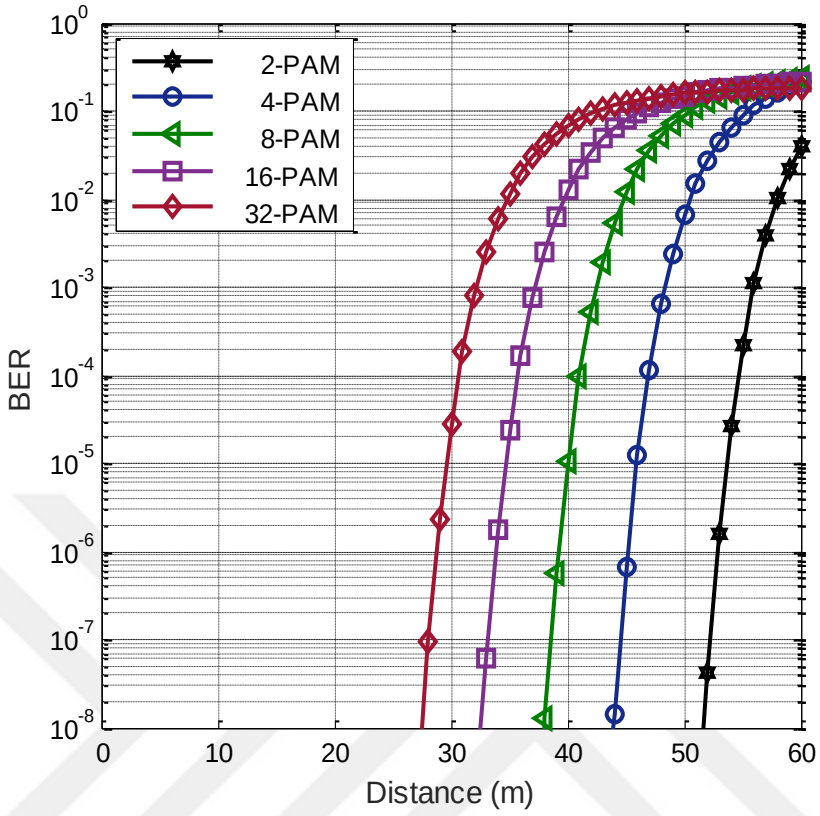

Figure 4: BER performance of V2V transmission for foggy weather with $V = 50$ m

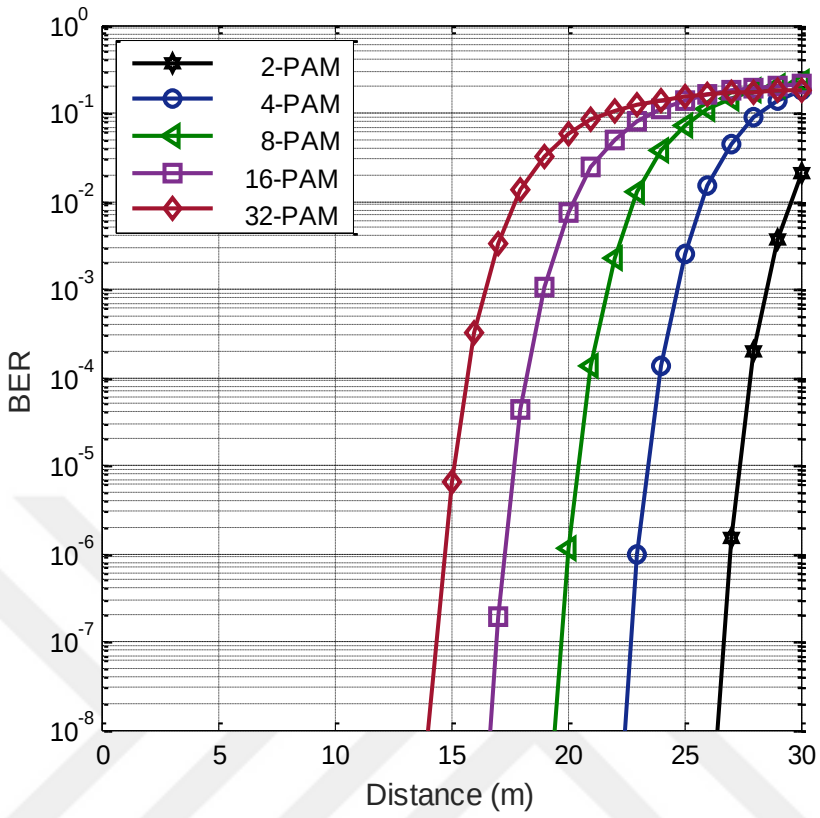

Figure 5: BER performance of V2V transmission for foggy weather with $V = 10$ m

Table 3: Maximum achievable distance for different weather types ($P_e' = 10^{-6}$)

Modulation	**Maximum Distance (m)**			
	Clear	**Rain**	**Fog, $V = 50$ m**	**Fog, $V = 10$ m**
2-PAM	72.21	69.13	52.85	26.93
4-PAM	61.49	58.88	45.12	23.01
8-PAM	53.23	50.98	39.17	19.98
16-PAM	45.81	43.88	33.81	17.25
32-PAM	38.73	37.11	28.71	14.66

In Figs. 6-9, the maximum achievable distance versus the number of relays for various weather conditions is presented. As a benchmark, direct transmission ($N = 0$) is included as well. It is observed that relaying significantly extends the transmission range. Assuming the deployment of single relay (i.e., $N = 1$) and 2-PAM, the achievable distance in clear weather, rainy weather, foggy weather with visibility of $V = 50$ m and foggy weather with visibility of $V = 10$ m increases to 137.01 m, 131.20 m, 100.40 m and 51.15 m. For $N = 10$ relays, this further increases to 654.01 m, 626.30 m, 480.20 m and 244.80 m. It is clear from the figure that a linear increase in transmission distance is not obtained. To better illustrate this, we obtain the improvement factor, i.e., $d_{\text{MH-PIN}}/d_{\text{PIN}}$, where d_{PIN} denotes the maximum achievable link distance for point-to-point communication link (i.e., $N = 0$). It is observed that the improvement factors for clear weather by 2-PAM at $N = 1$, 5 and 10 are respectively 1.89, 5.20 and 9.05. Expected improvement factor of ($N + 1$) is greater than these values. It can be further noted that improvement factors are also independent of the weather type. For example, at $N = 10$, we observe $d_{\text{MH-PIN}}/d_{\text{PIN}} = 9.05$, 9.05, 9.08, and 9.09 for clear weather, rainy weather, foggy weather with visibility of $V = 50$ m and foggy weather with visibility of $V = 10$ m, respectively.

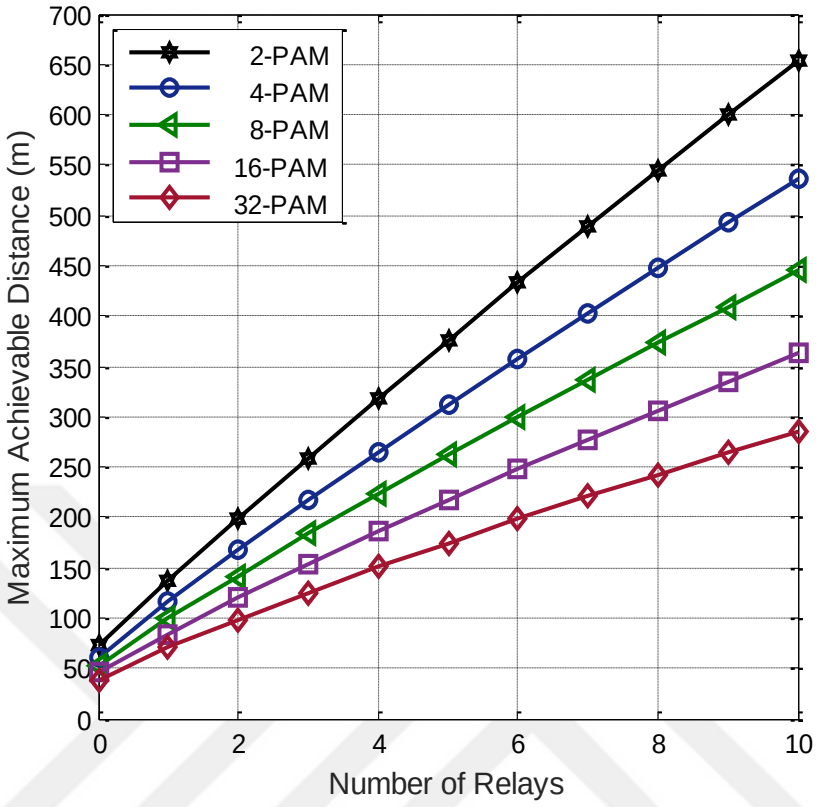

Figure 6: Maximum achievable distance versus number of relays for clear weather

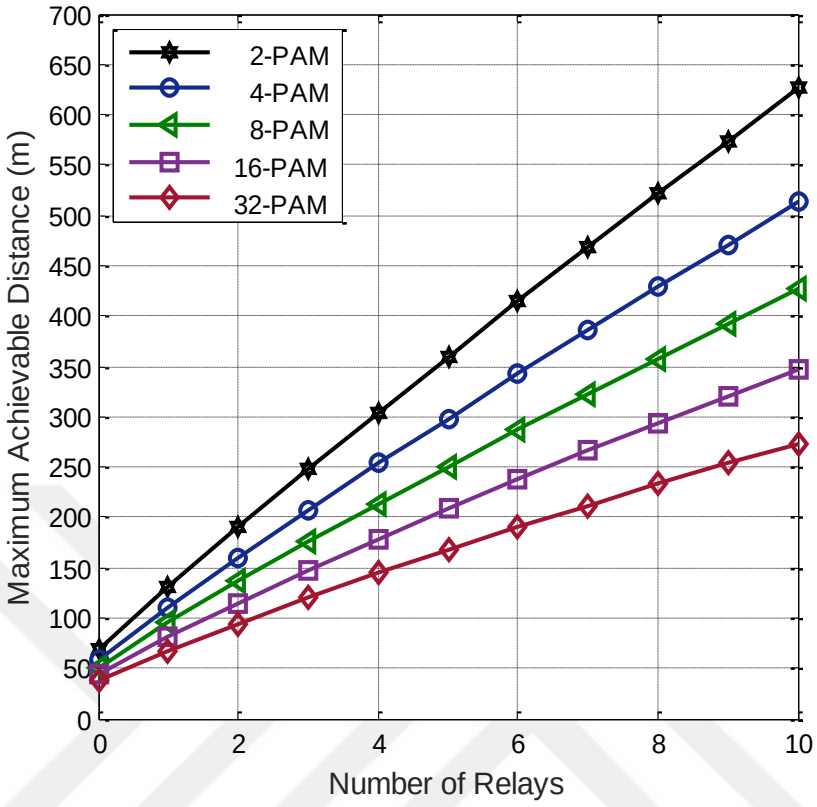

Figure 7: Maximum achievable distance versus number of relays for rainy weather

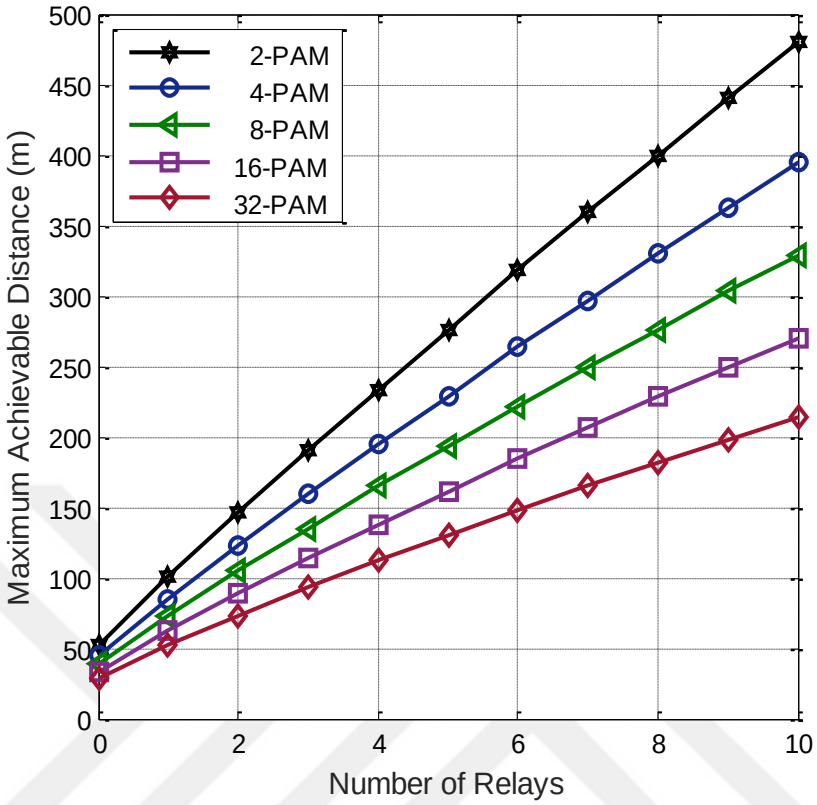

Figure 8: Maximum achievable distance versus number of relays for foggy weather with $V = 50$ m

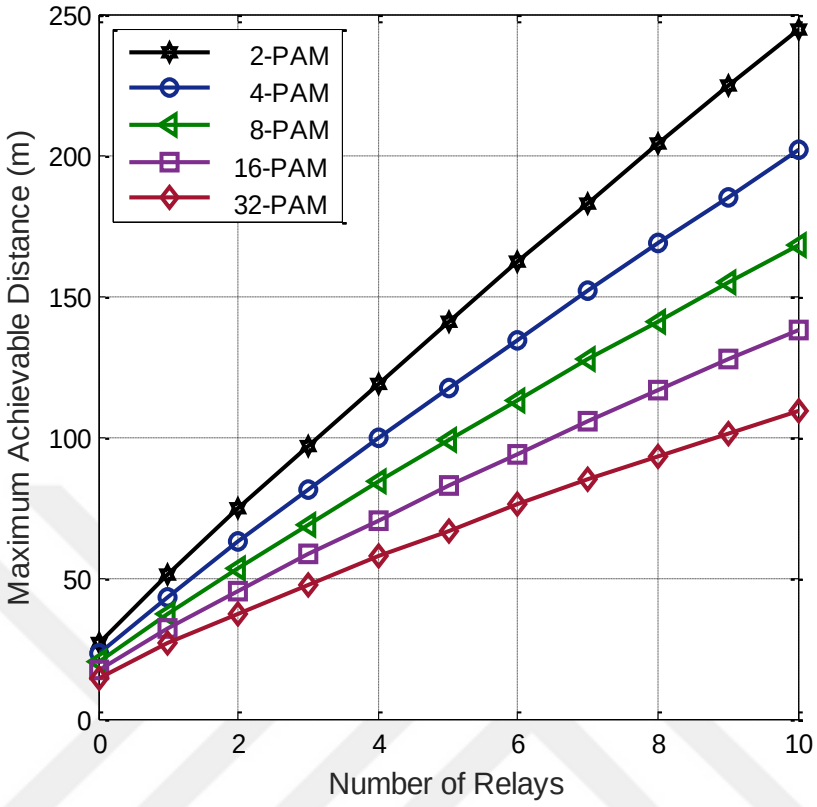

Figure 9: Maximum achievable distance versus number of relays for foggy weather with $V = 10$ m

CHAPTER III

Vehicular VLC with SPAD Receivers

In this chapter, we consider a V2V VLC system with SPAD receivers. We first derive a closed-form expression for BER. Then, using BER expression, we determine the maximum achievable distance between two vehicles to ensure targeted BER. We also investigate multi-hop transmission to extend transmission ranges. We further quantify performance improvements over conventional vehicular V2V VLC systems with APD receivers.

3.1 System Model

In this section, OOK is employed to modulate the light emitted from the LEDs with an average optical power of P_0. When bit '0' is transmitted, the transmit power is set as $P_t = 0$. On the other hand, when bit '1' is transmitted, the transmit power is set as $P_t = 2P_0$. The number of received photons is given by [27]

$$z = \eta P_t h T_b + \left(N_{DCR} + N_b \right) T_b \tag{10}$$

where T_b is the bit time duration and N_{DCR} is the dark count ratio of SPAD and N_b is the background light noise ratio. In (10), η is defined as

$$\eta = \frac{C_{PDE} \lambda}{h_{\text{Planck}} \nu} \tag{11}$$

where C_{PDE} is the photon detection efficiency, λ is the wavelength, h_{Planck} is the Planck's constant and v is the speed of light. In (10), h denotes the deterministic channel coefficient between two vehicles and is defined in (2).

The output photon number of SPAD receiver can be statistically modeled with Poisson distribution. The probability mass function is expressed as

$$\Pr(z) = \frac{\mu^z}{z!} e^{-\mu} \tag{12}$$

where $\mu = E(z)$ denotes the mean of received photon numbers. When bit '0' and bit '1' are transmitted, the mean received photon numbers are $\mu_0 = (N_{DCR} + N_b)T_b$ and $\mu_1 = \eta P_t h T_b + \mu_0$, respectively. Under the assumption that the message signals are equal likely, the optimum detection threshold is the intersection point of curves $\Pr(z, \mu_0)$ and $\Pr(z, \mu_1)$ as

$$\frac{\mu_0^{\ z}}{z!} e^{-\mu_0} = \frac{\mu_1^{\ z}}{z!} e^{-\mu_1} \tag{13}$$

Then, the optimum detection threshold can be obtained as

$$z_{\text{th}} = \frac{\eta P_t h T_b}{\ln\left(1 + \eta P_t h / (N_{DCR} + N_b)\right)} \tag{14}$$

3.2 Maximum Achievable Distance

3.2.1 Point-to-Point Transmission

In this section, we determine the maximum achievable distance to satisfy a targeted BER. BER for OOK under Poisson distribution can be written as [37]

$$\begin{aligned} P_e &= \frac{1}{2}\Pr\{z > z_{\text{th}} \mid 0\} + \frac{1}{2}\Pr\{z < z_{\text{th}} \mid 1\} \\ &= \frac{1}{2}\sum_{z=z_{\text{th}}+1}^{\infty} \frac{\mu_0^z}{z!} e^{-\mu_0} + \frac{1}{2}\sum_{z=0}^{z_{\text{th}}} \frac{\mu_1^z}{z!} e^{-\mu_1}. \end{aligned} \tag{15}$$

In an effort to find a closed-form BER expression, we use Anscombe root transformation [38-40] to approximate the Poisson noise by square-root additive white Gaussian noise (AWGN).

Given a random variable z obeying the Poisson distribution with mean $E(z)$, the Anscombe root transformation can be expressed as [38-40]

$$\hat{z} = 2\sqrt{z + 3/8} \tag{16}$$

According to [38-40], the variance of $\hat{z}$ is approximated by

$$\text{Var}\left(\hat{z}\right) \approx 1 + \frac{1}{16E^2(z)} \tag{17}$$

Based on (16), (17) and noting that $\text{Var}\left(\hat{z}\right) = E\left(\hat{z}^2\right) - E^2\left(\hat{z}\right)$, we obtain

$$E\left(4z + \frac{3}{2}\right) - E^2\left(\hat{z}\right) = 1 + \frac{1}{16E^2(z)} \tag{18}$$

and then, the mean of $\hat{z}$ can be then obtained as

$$E\left(\hat{z}\right) \approx 2\sqrt{E\left(z\right)+\frac{1}{8}-\frac{1}{48E^2\left(z\right)}} \tag{19}$$

According to [39], when $E\left(z\right)$ is large enough (i.e., should be larger than 4), $\hat{z}$ can be well approximated by a Gaussian variable with mean $E\left(\hat{z}\right) \approx 2\sqrt{E\left(z\right)+3/8}$ and unit variance. Therefore, P_e in (15) can be approximated as

$$\begin{aligned} P_e &\approx \frac{1}{2}\Pr\left\{\hat{z} > \delta \mid 0\right\} + \frac{1}{2}\Pr\left\{\hat{z} < \delta \mid 1\right\} \\ &= Q\left(\sqrt{\mu_1+\frac{3}{8}} - \sqrt{\mu_0+\frac{3}{8}}\right) \end{aligned} \tag{20}$$

where δ is the maximum likelihood (ML) threshold for signal $\hat{z}$ and can be obtained as

$$\delta = \sqrt{\mu_0+3/8} + \sqrt{\mu_1+3/8} \tag{21}$$

Let P_e' denote the targeted BER value. Solving (18) for h in (2), we have

$$h \approx \left(\frac{1}{\eta P_t T_b}\right)\left(\left(Q^{-1}\left(P_e'\right)+\sqrt{\mu_0+3/8}\right)^2 - \left(\mu_0+3/8\right)\right) \tag{22}$$

By replacing (2) in (22), the maximum transmission distance to satisfy P_e' is obtained as

$$d_{\text{SPAD}} \approx \left(\frac{1}{A}\right)\left(\left(10\log_{10}\left(\left(\frac{1}{P_t T_b \eta}\right)\left(\left(Q^{-1}\left(P_e'\right)+\sqrt{\mu_0+3/8}\right)^2 - \left(\mu_0+3/8\right)\right)\right)\right) - B\right) \tag{23}$$

3.2.2 Multi-Hop Transmission

In this section, we explore the deployment of multi-hop transmission to extend transmission range. We assume the deployment of DF relaying. Let N denote the number of relay terminals. As we proved in Section 2.2.2, the approximate upper bound on the maximum achievable distance through DF multi-hop transmission can be obtained by multiplying the maximum achievable distance per hop with $(N+1)$. Therefore, we can obtain

$$d_{\text{MH-SPAD}} \tilde{<} (N+1)\left(\frac{1}{A}\right) \times \left(\left(10\log_{10}\left(\left(\frac{\sqrt{(N+1)}}{P_t T_b \eta}\right)\left(\left(Q^{-1}\left(\frac{P'_{e,\text{SD}}}{N+1}\right)+\sqrt{\mu_0+3/8}\right)^2-(\mu_0+3/8)\right)\right)\right)-B\right) \quad (24)$$

3.3 Numerical Results

In this section, we first present numerical results for the BER to validate the accuracy of Anscombe transformation. Then we compare the achievable distance of vehicular VLC systems with SPAD and APD receivers under different weather conditions in both point-to-point and multi-hop scenarios. The BER performance of VLC systems with APD receiver is provided in Appendix. The simulation parameters are summarized in Tables 4 and 5. Since white LED headlamps are used in vehicular applications, η in (11) is calculated based on an average over the wide spectrum of visible band (400 nm-700 nm).

Table 4: SPAD parameters

Parameters	Values
Wavelength of light (λ)	400-700 nm
Speed of light (v)	3×10^8 m/s
Bit time duration (T_b)	1 ms [25]
The PDE of the SPAD (C_{PDE})	20% [29]
The DCR of the SPAD (N_{DCR})	7.27 kHz [29]

Table 5: APD parameters

Parameters	Values
Responsivity of the photodetector (r)	0.28 A/W [25]
Gain of photodetector (g)	50 [27]
Noise power spectral density (N_0)	10^{-22} W/Hz [25]

In Figs. 10-13, we compare the exact BER expression in (15) and the derived approximate BER expression in (20) assuming different weather types. The accuracy of approximation mainly depends on the mean value of Poisson random variable, i.e., $E(z)$, which should be sufficiently large. As introduced in Section 3.2.1, $E(z)$ is a function of SPAD dark count ratio (N_{DCR}), background light noise ratio (N_b), bit time duration (T_b), transmit power (P_t), channel coefficient (h) and the parameter η defined in (11). It can be readily verified that the mean is always sufficiently large for the simulation parameters under consideration. Therefore, the proposed approximation provides an excellent match for all transmission distances and transmit powers under consideration.

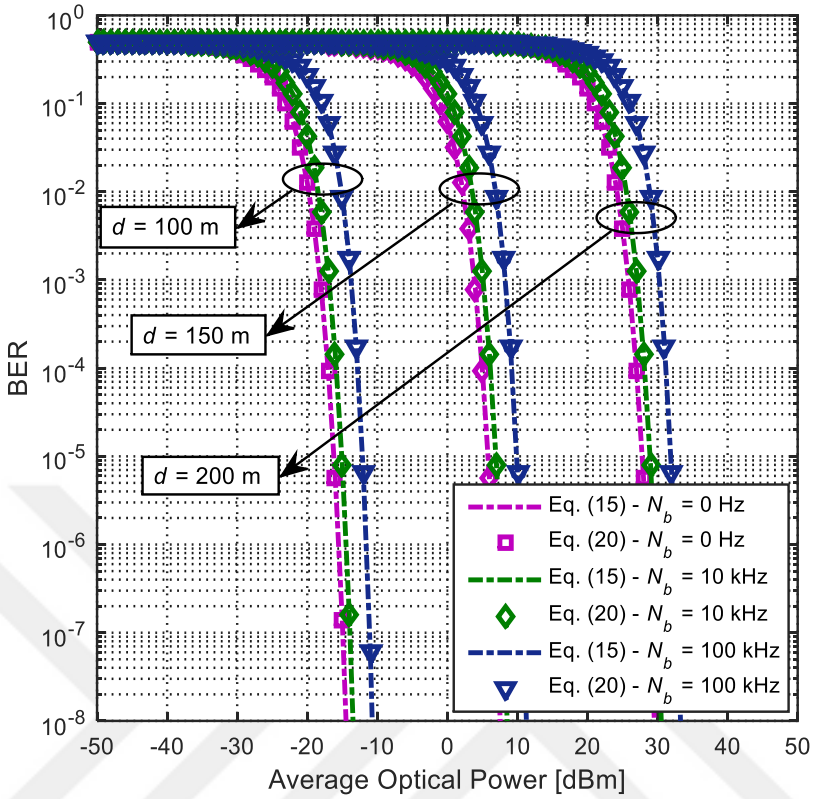

Figure 10: Comparison of the exact BER expression in (15) and the derived BER expression in (20) assuming clear weather

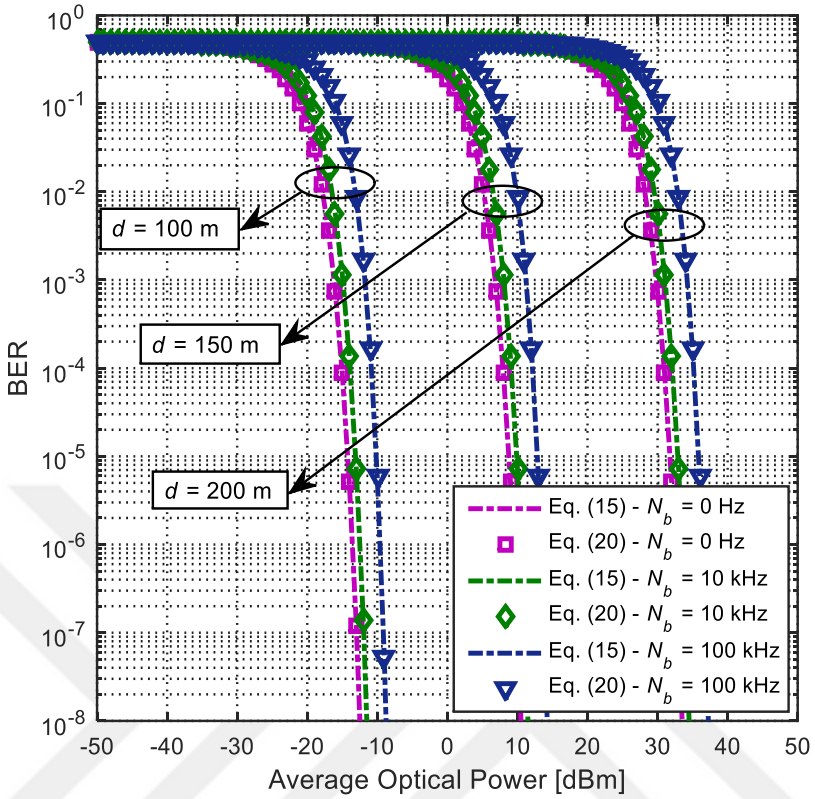

Figure 11: Comparison of the exact BER expression in (15) and the derived BER expression in (20) assuming rainy weather

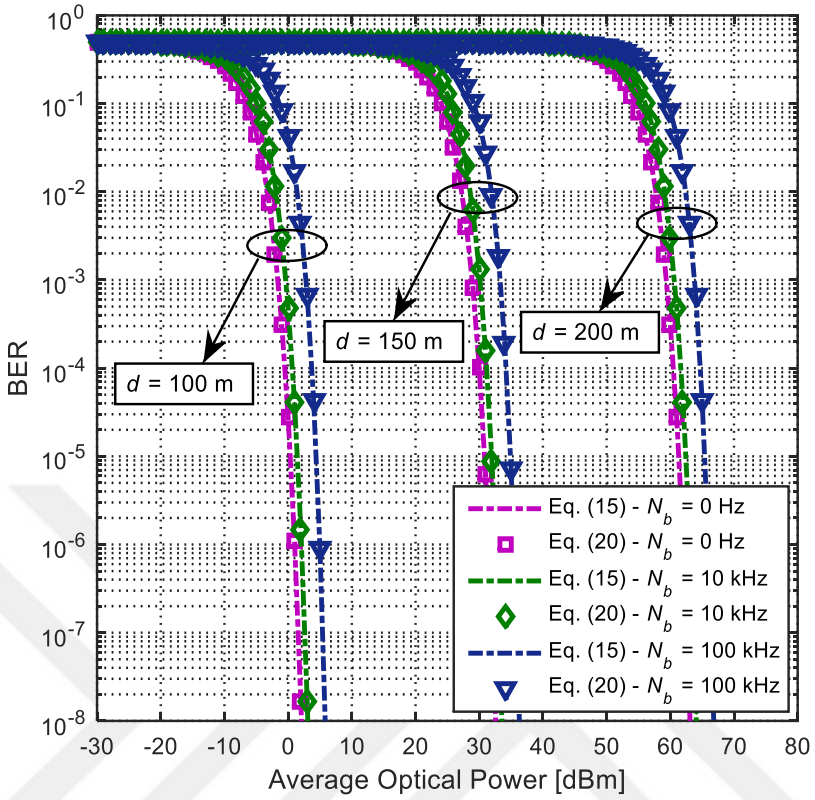

Figure 12: Comparison of the exact BER expression in (15) and the derived BER expression in (20) assuming foggy weather with V=50 m

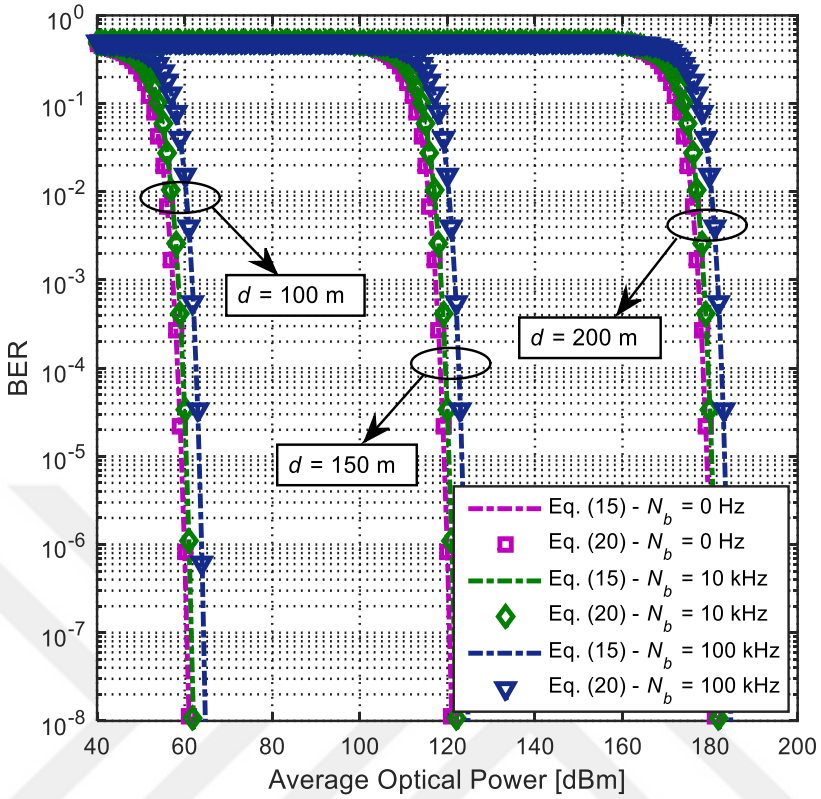

Figure 13: Comparison of the exact BER expression in (15) and the derived BER expression in (20) assuming foggy weather with V=10 m

In Fig. 14, based on (20) and (38), we present a BER performance comparison between SPAD and APD receivers at a fixed distance of 100 m. It is observed that the SPAD receiver provides a significant gain over APD receiver in all weather conditions under consideration. Specifically, at a BER target of $P_e' = 10^{-6}$, SPAD provides a ~30 dBm improvement over APD.

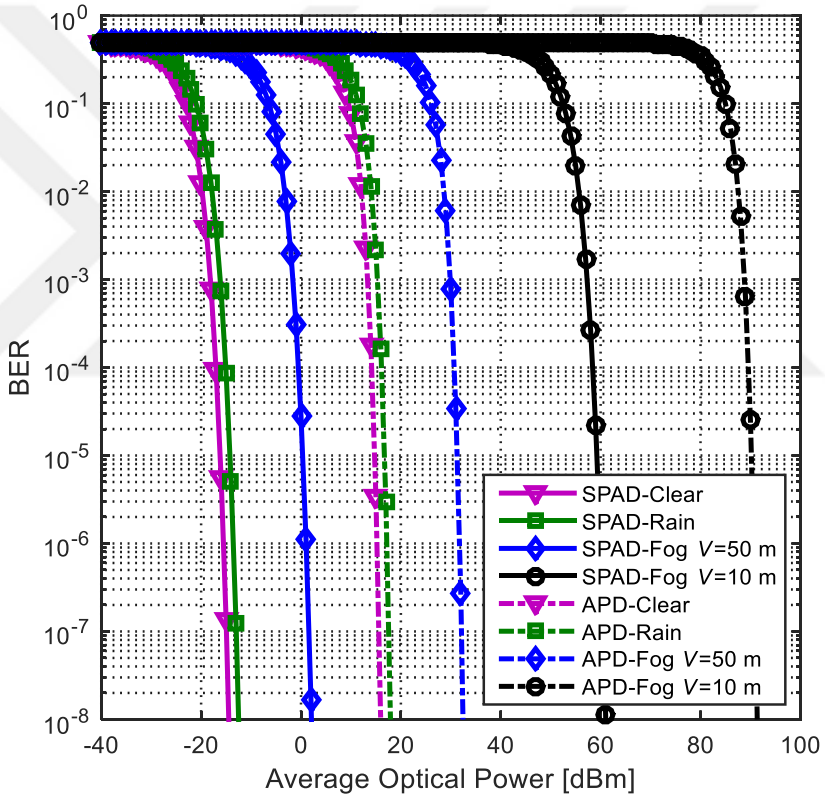

Figure 14: BER of SPAD- and APD-based V2V VLC transmission under different weather conditions

In Fig. 15, we present the maximum achievable distances for SPAD and APD receivers based on (23) and (39) at a targeted BER of $P_e' = 10^{-6}$. Here, we vary optical power from 0 dBm to 50 dBm. For example, at 20 dBm, it is observed that the maximum distance for SPAD receiver in clear weather is 180.70 m. This slightly reduces to 172.90 m in rainy weather. The fog, on the other hand, has severe impact. For a foggy condition with visibility $V = 50$ m, the achievable distance is 131.10 m. It becomes 66.71 m for a foggy weather with visibility of $V = 10$ m. For APD receiver, the achievable distances for clear, rainy and foggy weathers with visibilities of $V = 50$ m and $V = 10$ m respectively decrease to 110.80 m, 106.10 m, 80.71 m and 41.09 m. This indicates about 1.62 times improvement over the distances achievable by SPAD.

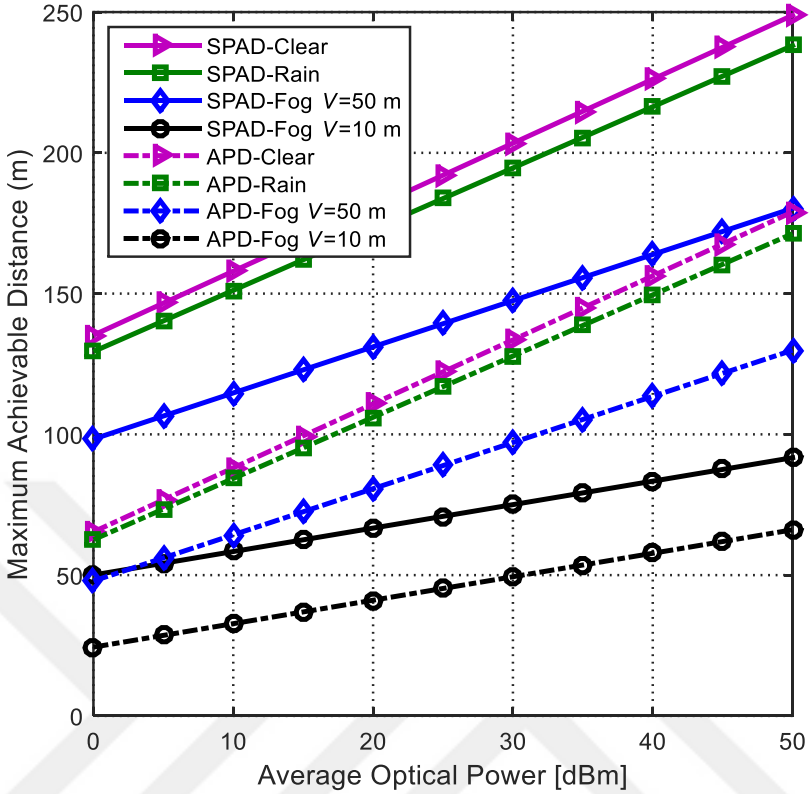

Figure 15: Maximum achievable distance for SPAD- and APD-based V2V VLC transmission under different weather conditions

In Fig. 16, the maximum achievable distance versus the number of relays for various weather conditions assuming SPAD receiver is presented. As a benchmark, direct transmission ($N=0$) is included as well. It is observed that relaying significantly extends the transmission range. Assuming the deployment of single relay (i.e., $N=1$), the achievable distance in clear weather, rainy weather, foggy weather with visibility of $V=$ 50 m and foggy weather with visibility of $V=10$ m increases to 353.70 m, 338.40 m, 256.70 m and 130.60 m. For $N=5$ relays, this further increases to 1025 m, 980.60 m, 743.80 m and 378.50 m. It is clear from the figure that a linear increase in transmission distance is not obtained. To better illustrate this, we obtain the improvement factor, i.e., $d_{\text{MH-SPAD}}/d_{\text{SPAD}}$, where d_{SPAD} denotes the maximum achievable link distance for point-to-point communication link (i.e., $N=0$). It is observed that the improvement factors for clear weather at $N=1$, 3 and 5 are respectively 1.95, 3.83 and 5.67. Expected improvement factor of ($N+1$) is greater than these values. It can be further noted that improvement factors are also independent of the weather type. For example, at $N=5$, we observe $d_{\text{MH-SPAD}}/d_{\text{SPAD}}=5.67$, 5.67, 5.67, and 5.67 for clear weather, rainy weather, foggy weather with visibility of $V=50$ m and foggy weather with visibility of $V=10$ m, respectively.

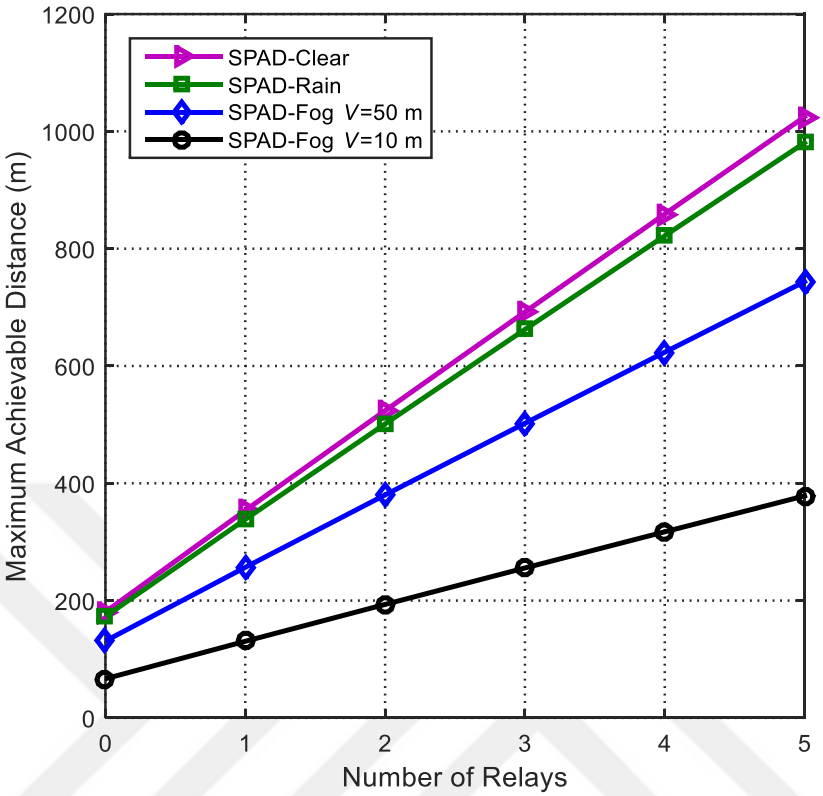

Figure 16: Maximum achievable distance versus number of relays for SPAD-based V2V VLC transmission under different weather conditions

CHAPTER IV

Vehicular VLC with SPAD Array Receivers

In this chapter, we consider V2V VLC system with SPAD array receivers using new path loss model between two vehicles. We derive maximum achievable distance between two vehicles to ensure targeted BER. We further present the effects of SPAD array and channel parameters on the maximum achievable distance.

4.1 System Model

We assume the deployment of OOK to modulate the light emitted from the LEDs with an average optical power of P_0 and bit time duration T_b. The power is set as $P_t = 0$ and $P_t = 2P_0$, respectively for transmitting zero and ones. Let N_{SPAD} and C_{FF} denote respectively the size and the fill factor (FF) of the SPAD array. The number of received photons is given by [27]

$$z = N_{SPAD} C_{FF} \left(\eta P_t h + N_{DCR} + N_b \right) T_b \tag{25}$$

where N_{DCR} is the dark count ratio, N_b is the background light noise ratio and $\eta = C_{PDE}\lambda / h_{\text{Planck}} v$. Here, C_{PDE} is the photon detection efficiency, λ is the wavelength, h_{Planck} is the Planck's constant and v is the speed of light. The channel coefficient h can be expressed as [41]

$$h = \left(\frac{D_R}{\zeta d} \right)^2 e^{-cd\left(\frac{D_R}{\zeta d}\right)^{\zeta}} \tag{26}$$

where D_R is the diameter of receive aperture. c stands for the extinction coefficient (summation of absorption and the scattering coefficients) for a specific weather type. In (26), ζ is defined as a correction coefficient introduced due to asymmetrical pattern of headlamp. The value of this correction coefficient depends on weather type. Corresponding ζ values are summarized in Table 6.

Poisson distribution is widely used to statistically model the SPAD receiver. The probability mass function of the output photon numbers is given by $\Pr(z) = \mu^z e^{-\mu} / z!$ where $\mu = E(z)$ denotes the mean of received photon numbers. The received photon numbers for the transmission of zero and ones are then calculated as $\mu_0 = N_{SPAD} C_{FF} (N_{DCR} + N_b) T_b$ and $\mu_1 = N_{SPAD} C_{FF} \eta P_t h T_b + \mu_0$, respectively. For equally likely message signals, it can be shown that the optimum detection threshold is $z_{\text{th}} = (\mu_1 - \mu_0) / \ln(\mu_1 / \mu_0)$.

4.2 Maximum Achievable Distance

BER for OOK under Poisson distribution can be then written as [37]

$$P_e = \frac{1}{2} \sum_{z=z_{\text{th}}+1}^{\infty} \frac{\mu_0^z}{z!} e^{-\mu_0} + \frac{1}{2} \sum_{z=0}^{z_{\text{th}}} \frac{\mu_1^z}{z!} e^{-\mu_1} \tag{27}$$

Using Gaussian approximation [42], the BER expression can be expressed as

$$P_e \approx Q\left(\frac{\mu_1 - \mu_0}{\sqrt{\mu_1} + \sqrt{\mu_0}} \right) \tag{28}$$

We specify the maximum achievable distance to ensure targeted BER as following. First we obtain d in respect to h and channel parameters from (26). After doing some mathematical utilization on (26), we can write

$$(1-\zeta)\left(\frac{c}{2}\frac{D_R^{\zeta}}{\zeta^{\zeta}}\right)d^{(1-\zeta)}e^{(1-\zeta)\left(\frac{c}{2}\frac{D_R^{\zeta}}{\zeta^{\zeta}}\right)d^{(1-\zeta)}} = (1-\zeta)\left(\frac{c}{2}\frac{D_R^{\zeta}}{\zeta^{\zeta}}\right)\left(\frac{h\zeta^2}{D_R^2}\right)^{\left(\frac{\zeta-1}{2}\right)} \tag{29}$$

Since the left-hand side of aforementioned expression has a form of xe^x, we can use the Lambert-W function [43] to find its inverse. Let $\mathrm{W}\left(xe^x\right)=x$ denote the Lambert-W function. From (29), d can be obtained as

$$d = \left(\frac{\mathrm{W}\left(\frac{c}{2}(1-\zeta)\left(\frac{D_R}{\zeta}\right)h^{\left(\frac{\zeta-1}{2}\right)}\right)}{\frac{c}{2}(1-\zeta)\left(\frac{D_R}{\zeta}\right)^{\zeta}}\right)^{\frac{1}{1-\zeta}} \tag{30}$$

Let P_e' denote the targeted BER value. To solve (28) for h in (26), we first solve (28) for μ_1. By taking inverse *Q*-function from both sides of (28), we have

$$Q^{-1}\left(P_e'\right) \approx \frac{\mu_1-\mu_0}{\sqrt{\mu_1}+\sqrt{\mu_0}} \tag{31}$$

By re-arranging (31), we have

$$\mu_1 - Q^{-1}\left(P_e'\right)\sqrt{\mu_1} - \left(Q^{-1}\left(P_e'\right)\sqrt{\mu_0}+\mu_0\right) \approx 0 \tag{32}$$

The left-hand side of (32) has a form of $\alpha x^2+\beta x+\gamma$ where $x=\sqrt{\mu_1}$, $\alpha=1$, $\beta=-Q^{-1}\left(P_e'\right)$ and $\gamma=-\left(Q^{-1}\left(P_e'\right)\sqrt{\mu_0}+\mu_0\right)$. The roots of this quadratic equation can be found as $x=\left(-\beta\pm\sqrt{\beta^2-4\alpha\gamma}\right)\Big/2\alpha$ [44]. Therefore, we have

$$\mu_1\approx\sqrt{\frac{Q^{-1}\left(P_e'\right)+\sqrt{\left(Q^{-1}\left(P_e'\right)\right)^2+4\left(Q^{-1}\left(P_e'\right)\sqrt{\mu_0}+\mu_0\right)}}{2}} \tag{33}$$

Based on (33) and noting that $\mu_1=N_{SPAD}C_{FF}\eta P_t hT_b+\mu_0$, we have

$$N_{SPAD}C_{FF}\eta P_t hT_b+\mu_0\approx\left(\frac{Q^{-1}\left(P_e'\right)+\sqrt{\left(Q^{-1}\left(P_e'\right)\right)^2+4\left(Q^{-1}\left(P_e'\right)\sqrt{\mu_0}+\mu_0\right)}}{2}\right)^2 \tag{34}$$

By re-arranging (34), we can obtain h as

$$h\approx\frac{1}{N_{SPAD}C_{FF}\eta P_t T_b}\left(\frac{1}{4}\left(Q^{-1}\left(P_e'\right)+\sqrt{\left(Q^{-1}\left(P_e'\right)\right)^2+4\left(Q^{-1}\left(P_e'\right)\sqrt{\mu_0}+\mu_0\right)}\right)^2-\mu_0\right) \tag{35}$$

By replacing (35) in (30), the maximum achievable link distance to achieve P_e' can be obtained as

$$d \approx \left(\frac{\mathrm{W}\left(\frac{c}{2}(1-\zeta)\left(\frac{D_R}{\zeta}\right)\left(\frac{1}{N_{SPAD} C_{FF} \eta P_t T_b}\left(\frac{1}{4}\left(Q^{-1}\left(P_e'\right) + \sqrt{\left(Q^{-1}\left(P_e'\right)\right)^2 + 4\left(Q^{-1}\left(P_e'\right)\sqrt{\mu_0} + \mu_0\right)}\right)^2 - \mu_0 \right)\right)^{\left(\frac{\zeta-1}{2}\right)} \right)}{\frac{c}{2}(1-\zeta)\left(\frac{D_R}{\zeta}\right)^{\zeta}} \right)^{\frac{1}{1-\zeta}}$$

(36)

4.3 Numerical Results

In this section, we present numerical results for the maximum achievable link distance under different weather conditions and system parameters to achieve a specified BER. Unless otherwise stated, we assume $P_t = $ -50 dBm [29], receiver aperture diameter of $D_R = 5$ cm, fill factor of $C_{FF} = 0.5$ [45], array size of $N_{SPAD} = 8\times8$ [42] and $N_{DCR} =$ 7.27 kHz [29]. The simulation parameters are summarized in Table 6. Since white LED headlamps are used in vehicular applications, η is calculated based on an average over the wide spectrum of visible band (400 nm-700 nm).

Table 6: Configurations under consideration

	$D_R = 1$ cm	$D_R = 3$ cm	$D_R = 5$ cm	$D_R = 10$ cm	$D_R = 15$ cm
Clear Weather	0.1618	0.1650	0.1650	0.1647	0.1648
Rain	0.1699	0.1706	0.1703	0.1699	0.1697
Moderate Fog	0.1678	0.1658	0.1655	0.1633	0.1620
Thick Fog	0.1725	0.1722	0.1686	0.1637	0.1618

Table 7: Simulation parameters

Parameters	Value
Wavelength of light (λ)	400 nm-700 nm
Speed of light (v)	3×10^8 m/s
Bit time duration (T_b)	1 μs
The PDE of the SPAD (C_{PDE})	20% [29]
The DCR of the SPAD (N_{DCR})	7.27 kHz [29]
The FF of the SPAD (C_{FF})	0.5 [29]
Size of the SPAD (N_{SPAD})	8×8 [42]

In Fig. 17, we present the achievable V2V distance assuming clear weather, rain and fog for the above system configuration. It is observed that a transmission range of 34.15 m is possible for clear weather at $P_e' = 10^{-6}$. This slightly reduces to 33.08 m in rain. On the other hand, for foggy condition, the achievable distances are 32.12 m and 30.01 m for moderate fog and thick fog, respectively.

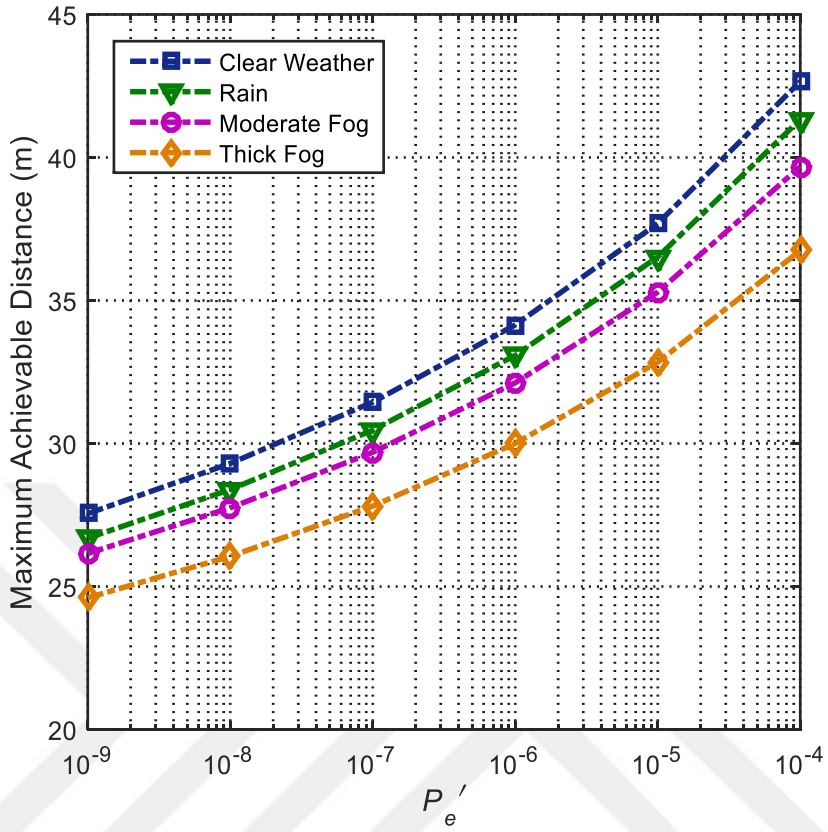

Figure 17: Maximum achievable distance under different weather conditions

In Fig. 18, we present the maximum achievable V2V distance assuming different values of receiver aperture diameter. We consider thick fog. Our results reveal that the maximum achievable distance increases with the increase in receiver aperture diameter increases. This is expected because a receiver with larger aperture is able to collect more energy. Mathematically speaking, the maximum achievable distance at $P_e' = 10^{-6}$ is 6.39 m for $D_R = 1$ cm. This increases to 18.4 m, 30.01 m, 55.87 m and 77.64 m for $D_R = 3$ cm, $D_R = 5$ cm, $D_R = 10$ cm and $D_R = 15$ cm, respectively. According to EU Member States regulations, a safe trailing distance of 28 m should be maintained between two vehicles based on 2-second rule assuming a travelling speed of 50 km/h [46]. Therefore, the aperture size of $D_R = 5$ cm is selected in the rest of this study.

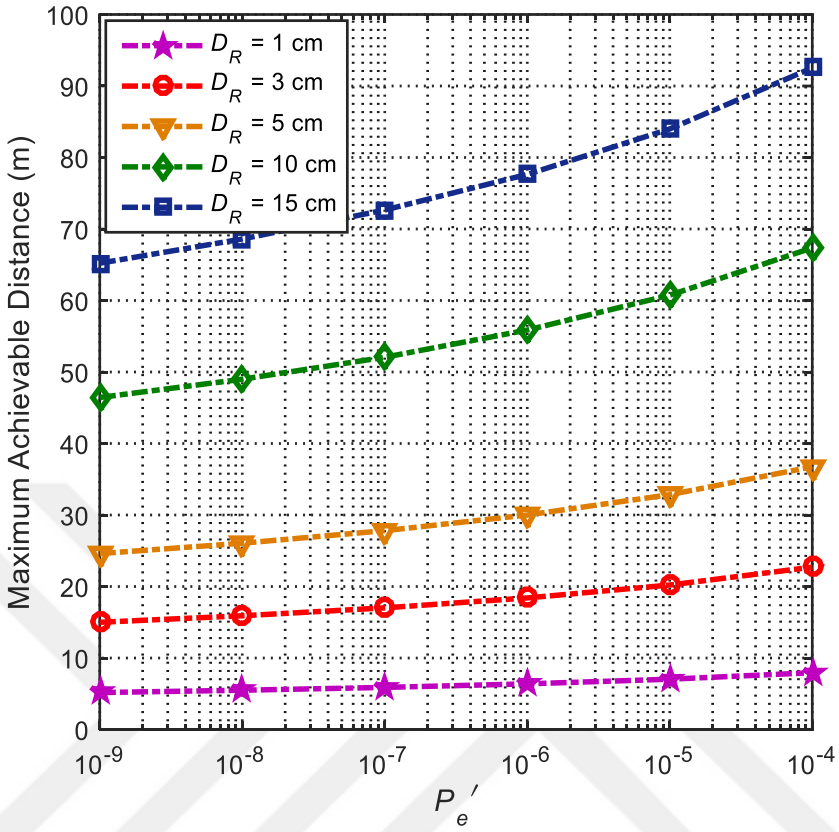

Figure 18: Maximum achievable distance assuming different receiver aperture diameters

In Fig. 19, we investigate the effect of background light noise ratio on the maximum achievable V2V distance. Here, we consider thick fog and vary background light noise ratio from much smaller than dark counts (i.e., at night with $N_b = 0$ Hz) to much bigger than dark counts during daylight (i.e., $N_b = 100$ kHz). It is observed that as background light noise ratio increases, the maximum achievable distance decreases. For example, under the assumption of $N_b = 0$ Hz and $P_e' = 10^{-6}$, a V2V distance of 30.01 m is achievable. This reduces to 28.82 m and 25.04 m for $N_b = 10$ kHz and $N_b = 100$ kHz, respectively.

In Fig. 20, we investigate the effect of SPAD parameters, i.e., fill factor and array size on the maximum achievable V2V distance. We consider thick fog. It is observed that as fill factor and array size increase, the maximum achievable distance increases. For $N_{\text{SPAD}} = 8\times8$ and $P_e' = 10^{-6}$, a distance of 30.01 m is achievable assuming a fill factor of $C_{FF} = 0.5$. This increases to 33.25 m and 39.86 m for $C_{FF} = 0.64$ [42] and $C_{FF} = 1$ (i.e., hypothetical case where the total array area is assumed to be active), respectively.

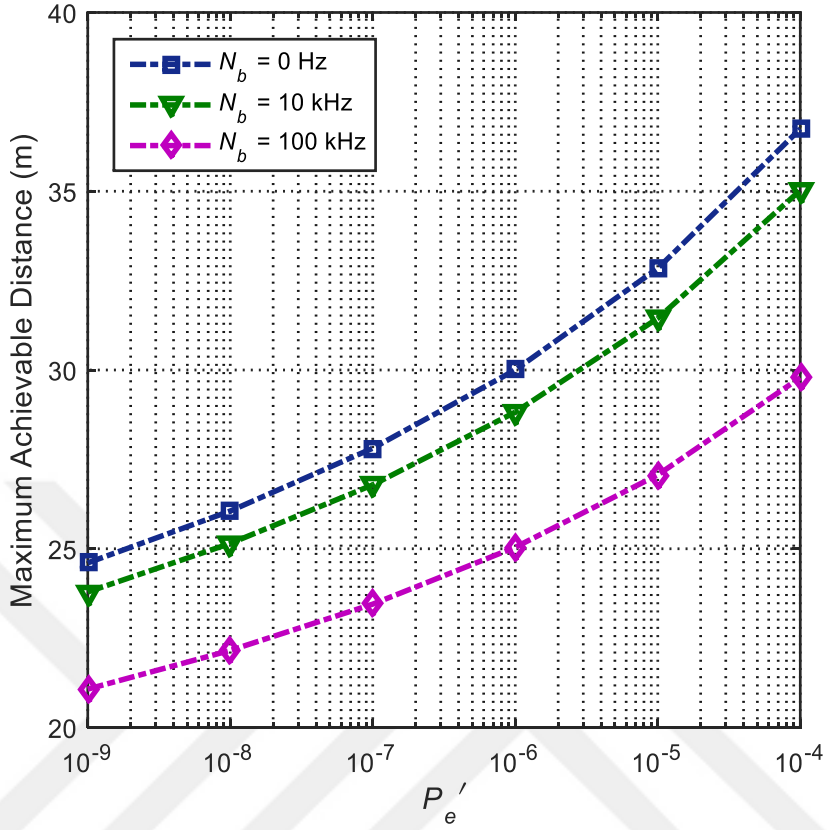

Figure 19: Maximum achievable distance assuming different background light noise ratios

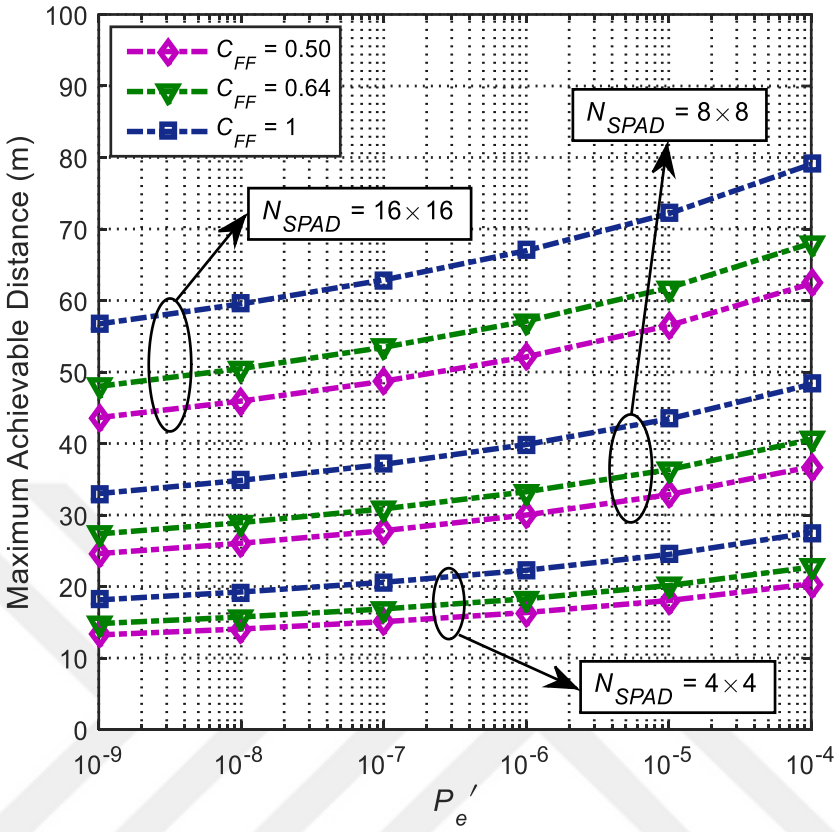

Figure 20: Maximum achievable distance for different SPAD array parameters (i.e., fill factor and size of the array)

CHAPTER V

CONCLUSIONS

In this thesis, we investigated the performance of a V2V VLC system with different receiver types including PIN-diode, SPAD and SPAD array receivers under various weather conditions.

In Chapter II, we investigated the performance of V2V VLC system with PIN-diode receiver and determined the maximum achievable distance to ensure a targeted BER. Our results indicated that for a typical system configuration and assuming the deployment of 2-PAM, the maximum achievable distance in clear weather conditions is about 72 m. This reduces to around 26 m in the presence of fog. We further investigated multi-hop transmission to extend transmission ranges

In Chapter III, we investigated the performance of V2V VLC system with SPAD receiver. Under OOK assumption, we first derived an approximate closed-form BER expression based on the Anscombe transformation, i.e., approximation of the Poisson noise by square-root AWGN. Then, we obtained the maximum achievable link distance to ensure a targeted BER under various weather conditions including rain and fog. We further quantified performance improvements over conventional vehicular V2V VLC systems with APD receivers. We further investigated multi-hop transmission to extend transmission ranges.

In Chapter IV, we used a new path loss model to derive a closed-form expression for the maximum achievable V2V distance. We considered the deployment of SPAD array as receiver where the output photon number is modeled with Poisson statistics. We determined the maximum achievable V2V distance to satisfy a targeted BER value. Our results demonstrated that, with proper selection of system parameters, VLC can provide a reliable connectivity solution for V2V links.

Appendix

As a benchmark, we consider a VLC system with APD receiver. Similar to SPAD receiver, when bit '0' is transmitted, the power of LED is $P_t = 0$, and when bit '1' is transmitted, the power of LED is $P_t = 2P_0$ where P_0 is the average transmitted optical power. The electrical received signal can be written as

$$y = grP_t hT_b + n \tag{37}$$

where g and r are the gain and responsivity of the photodetector, respectively. h denotes the deterministic channel coefficient which is defined in (2). T_b is the bit time duration and n is AWGN with zero mean and variance of σ_n^2. The BER of OOK for APD receiver can be written as

$$P_e \approx Q\left(\sqrt{\frac{\left(grhP_0\right)^2 T_b}{N_0}}\right) \tag{38}$$

where N_0 is the noise power spectral density. Let P_e' denote the targeted BER value. The maximum transmission distance for APD receiver in point-to-point transmission can be obtained by

$$d_{\text{APD}} \approx \left(\frac{1}{A}\right)\left(10\log_{10}\left(\left(\sqrt{\frac{N_0}{\left(grP_t\right)^2 T_b}}\right)Q^{-1}\left(P_e'\right)\right) - B\right) \tag{39}$$

where A and B are weather-dependent coefficients (see Table 1).

REFERENCES

[1] A. Perallos, U. Hernandez-Jayo, I. J. G. Zuazola, and E. Onieva, *Intelligent Transport Systems: Technologies and Applications.* John Wiley & Sons, 2015.

[2] F. A. Teixeira, V. F. e Silva, J. L. Leoni, D. F. Macedo, J. M. S. Nogueira, "Vehicular networks using the IEEE 802.11p standard: An experimental analysis", *Elsevier Vehicular Communications* vol. 1, no. (2), pp. 91–96, 2014.

[3] G. Araniti, C. Campolo, M. Condoluci, A. Iera, A. Molinaro, "LTE for vehicular networking: A survey", *IEEE Communications Magazine*, vol.51, no. 5, pp. 148-157, May 2013.

[4] R. Molina-Masegosa and J. Gozalvez, "LTE-V for sidelink 5G V2X vehicular communications: A new 5G technology for short-range vehicle-to-everything communications," *IEEE Vehicular Technology Magazine,* vol. 12, no. 4, pp. 30-39, Dec. 2017.

[5] T. Yamazato et al., "Image-sensor-based visible light communication for automotive applications," *IEEE Commun. Mag.,* vol. 52, no. 7, pp. 88–97, Jul. 2014.

[6] M. Uysal, Z. Ghassemlooy, A. Bekkali, A. Kadri and H. Menouar, "Visible light communication for vehicular networking: performance study of a V2V system using a measured headlamp beam pattern model," *IEEE Veh. Technol. Mag.,* vol. 10, no. 4, pp. 45-53, Dec. 2015.

[7] A. M. Cailean and M. Dimian, "Impact of IEEE 802.15.7 standard on visible light communications usage in automotive applications," *IEEE Communications Magazine,* vol. 55, no. 4, pp. 169-175, April 2017.

[8] A. T. Hussein, M. T. Alresheedi, and J. M. H. Elmirghani, "20 Gb/s mobile indoor visible light communication system employing beam steering and computer generated holograms," *J. Lightw. Technol.,* vol. 33, no. 24, pp. 5242–5260, Dec. 15, 2015.

[9] H. Chun *et al.*, "LED based wavelength division multiplexed 10 Gb/s visible light communications," *J. Lightw. Technol.,* vol. 34, no. 13, pp. 3047–3052, Jul. 1, 2016.

[10] S. Wu, H. Wang, and C.-H. Youn, "Visible light communications for 5G wireless networking systems: From fixed to mobile communications," *IEEE Netw.,* vol. 28, no. 6, pp. 41–45, Nov./Dec. 2014.

[11] C.-X. Wang *et al.*, “Cellular architecture and key technologies for 5G wireless communication networks,” *IEEE Commun. Mag.*, vol. 52, no. 2, pp. 122–130, Feb. 2014.

[12] M. B. Rahaim and T. D. C. Little, “Toward practical integration of dual-use VLC within 5G networks,” *IEEE Wireless Commun.*, vol. 22, no. 4, pp. 97–103, Aug. 2015.

[13] M. Ayyash *et al.*, “Coexistence of WiFi and LiFi toward 5G: Concepts, opportunities, and challenges,” *IEEE Commun. Mag.*, vol. 54, no. 2, pp. 64–71, Feb. 2016.

[14] X. Li, R. Zhang, and L. Hanzo, “Cooperative load balancing in hybrid visible light communications and WiFi,” *IEEE Trans. Commun.*, vol. 63, no. 4, pp. 1319–1329, Apr. 2015.

[15] *Fact Sheet 296—Electromagnetic Fields and Public Health*, World Health Org., Geneva, Switzerland, Dec. 2005.

[16] “IARC classifies radio frequency electromagnetic fields as possible carcinogenic to humans,” Int. Agency Res. Cancer, World Health Org., Geneva, Switzerland, Tech. Rep., May 2011, accessed on Mar. 20, 2017. [Online]. Available: http://www.iarc.fr/en/media-centre/ pr/2011/pdfs/pr208_E.pdf

[17] *Fact Sheet 193—Electromagnetic Fields and Public Health: Mobile Phones*, World Health Org., Geneva, Switzerland, Jun. 2011.

[18] *Fact Sheet 193—Electromagnetic Fields and Public Health: Mobile Phones, World Health Org., Geneva, Switzerland, Oct. 2014.*

[19] S. Kitano, S. Haruyama, and M. Nakagawa, “LED road illumination communications system,” in *Proc. 58th IEEE Veh. Technol. Conf. (VTC Fall)*, vol. 5. Orlando, FL, USA, Oct. 2003, pp. 3346–3350.

[20] N. Kumar, “Smart and intelligent energy efficient public illumination system with ubiquitous communication for smart city,” in *Proc. IEEE Int. Conf. Smart Struct. Syst. (ICSSS)*, Chennai, India, Mar. 2013, pp. 152–157.

[21] M. Ergen, “Critical penetration for vehicular networks,” *IEEE Commun. Lett.*, vol. 14, no. 5, pp. 414–416, May 2010.

[22] A. M. Căilean and M. Dimian, “Current challenges for visible light communications usage in vehicle applications: A survey,” *IEEE Communications Surveys & Tutorials*, vol. 19, no. 4, pp. 2681-2703, Fourthquarter 2017.

[23] Y. H. Kim, W. A. Cahyadi and Y. H. Chung, “Experimental demonstration of VLC-based vehicle-to-vehicle communications under fog conditions,” *IEEE Photonics Journal*, vol. 7, no. 6, pp. 1-9, Dec. 2015.

[24] A. M. Căilean, B. Cagneau, L. Chassagne, M. Dimian and V. Popa, "Novel receiver sensor for visible light communications in automotive applications," in *IEEE Sensors Journal,* vol. 15, no. 8, pp. 4632-4639, Aug. 2015.

[25] M. Elamassie, M. Karbalayghareh, F. Miramirkhani, R. C. Kizilirmak, and M. Uysal, "Effect of fog and rain on the performance of vehicular visible light communications", *IEEE 87th Vehicular Technology Conference (VTC2018-Spring),* Porto, Portugal, 2018.

[26] T. Shafique, O. Amin, M. Abdallah, I. S. Ansari, M. S. Alouini and K. Qaraqe, "Performance analysis of single-photon avalanche diode underwater VLC system using ARQ," *IEEE Photonics Journal,* vol. 9, no. 5, pp. 1-11, Oct. 2017.

[27] M. Karbalayghareh, F. Miramirkhani, M. Safari, and M. Uysal, "Vehicular visible light communications with SPAD receivers", *IEEE Wireless Communications and Networking Conference (WCNC'19),* Marrakech, Morocco, Apr. 2019.

[28] Y. Li, M. Safari, R. Henderson and H. Haas, "Nonlinear distortion in SPAD-based optical OFDM systems," *IEEE Globecom Workshops (GC Wkshps),* San Diego, CA, 2015, pp. 1-6.

[29] Y. Li, M. Safari, R. Henderson and H. Haas, "Optical OFDM with single-photon avalanche diode," in *IEEE Photonics Technology Letters,* vol. 27, no. 9, pp. 943-946, May1, 1 2015.

[30] C. Wang, H. Y. Yu, Y. J. Zhu and T. Wang, "Blind detection for SPAD-based underwater VLC system under P–G mixed noise model," in *IEEE Communications Letters,* vol. 21, no. 12, pp. 2602-2605, Dec. 2017.

[31] Y. Li, S. Videv, M. Abdallah, K. Qaraqe, M. Uysal and H. Haas, "Single photon avalanche diode (SPAD) VLC system and application to downhole monitoring," *IEEE Global Communications Conference,* Austin, TX, 2014, pp. 2108-2113.

[32] T. Fath, and H. Haas, "Performance comparison of MIMO techniques for optical wireless communications in indoor environment", *IEEE Trans. Commun.,* vol. 61, no. 2, pp. 733-742, 2013.

[33] E. Morgado, I. Mora-Jimenez, J. J. Vinagre, J. Ramos, and A. J. Caamano, "End-to-end average BER in multihop wireless networks over fading channels", *IEEE Trans. Wirel. Commun.,* vol. 9, no. 8, pp. 2478- 2487, 2010.

[34] A. Florea, and H. Yanikomeroglu, "On the optimal number of hops in infrastructure-based fixed relay networks", in *IEEE Global Telecommunications Conference (GLOBECOM 2005),* pp. 3242 3247, 2005.

[35] L. H. Sperling, *Introduction to physical polymer science,* John Wiley & Sons, 2005.

[36] J. Grubor, S. Randel, K. D. Langer, and J. W. Walewski, “Broadband information broadcasting using LED-based interior lighting”, *J. Lightwave Technol.,* vol. 26, no. 24, pp. 3883-3892, 2008.

[37] E. Sarbazi, M. Safari and H. Haas, “Statistical modeling of single-photon avalanche diode receivers for optical wireless communications,” in *IEEE Transactions on Communications.*

[38] M. S. Bartlett, “The square root transformation in analysis of variance,” *Journal of the Royal Statistical Society*, vol. 3, no. 1, pp. 68-78, 1936.

[39] P. H. Leslie, “The transformation of Poisson, binomial and negative-binomial data,” *Biometrika,* vol. 35, no. 3-4, pp. 246–254, 1948.

[40] J. Zhang, L. H. Si-Ma, B. Q. Wang, J. K. Zhang and Y. Y. Zhang, “Low-complexity receivers and energy-efficient constellations for SPAD VLC systems,” *IEEE Photonics Technology Letters,* vol. 28, no. 17, pp. 1799-1802, Sept.1, 1 2016.

[41] Mehdi Karbalayghareh, Farshad Miramirkhani, Hossein B. Eldeeb, Refik Caglar Kizilirmak, Sadiq M. Sait, and Murat Uysal, “Performance characterization of vehicular visible light communications” *submitted to IEEE Transactions on Vehicular Technology.*

[42] E. Sarbazi, M. Safari, and H. Haas, “Photon detection characteristics and error performance of SPAD array optical receivers”, in *4th International Workshop on Optical Wireless Communications (IWOW),* pp. 132-136, 2015.

[43] J. J. Shynk, *Mathematical foundations for linear circuits and systems in engineering,* Wiley, 2016.

[44] V. L. Zaguskin, *Handbook of numerical methods for the solution of algebraic and transcendental equations,* Elsevier, 1961.

[45] E. Fisher, I. Underwood, and R. Henderson, “A reconfigurable single-photon-counting integrating receiver for optical communications”, *IEEE J. Solid-State Circuits,* vol. 48, no. 7, pp. 1638-1650, 2013.

[46] https://ec.europa.eu/transport/road_safety/specialist/knowledge/speed/speed_limits/current_speed_limit_policies_en

VITA

Mehdi Karbalay Ghareh received his B.Sc. degree with high honors in Electrical Engineering from Iran University of Science and Technology (IUST), Tehran, Iran, in 2016. He is currently pursuing the M.Sc. degree with the Communication Theory and Technologies (CT&T) Research Group, Ozyegin University, Istanbul, Turkey. His current research interests include indoor, vehicular, and underwater visible light communications, orthogonal frequency division multiplexing (OFDM), orthogonal frequency division multiple access (OFDMA), cooperative communications, resource allocation, multi-input multi-output (MIMO) communications and energy harvesting.